Q. J. R. Meteorol. Soc. (2001), **127**, pp. 2153–2179

Retrieval of microphysical and morphological properties of volcanic ash plumes from satellite data: Application to Mt Ruapehu, New Zealand

By A. J. PRATA* and I. F. GRANT
CSIRO, Australia

(Received 16 May 2000; revised 23 January 2001)

SUMMARY

A quantitative analysis of the properties of several Mt Ruapehu, New Zealand, ash plumes has been performed using multispectral satellite data from the AVHRR-2 and ATSR-2 instruments. The analysis includes: identification of the plume from background clouds using the 'reverse' absorption effect in the thermal channels; modelling and retrieval of particle sizes; determination of the plume height from cloud shadows, stereoscopy and meteorological data; and estimates of the mass of fine particles (radii less than 10 μm). A new spectral technique for identifying opaque, silica-rich ash clouds is demonstrated by utilizing the near-infrared (1.6 μm) and visible (0.67 μm) channels of the ATSR-2, and the optical properties of a simple volcanic cloud are presented for use in radiative transfer studies. It is found that the Ruapehu eruption cloud contained silica-rich ash particles with radii generally less than a few micrometres. The distribution of fine particles is monomodal with a dominant mode peak of about 3 μm radius. Mass loadings of fine particles are found to be in the range $\approx$1 to $\approx$7 mg m^{-3}, and are consistent with estimates of mass loadings of volcanic clouds from eruptions of other volcanoes. The height of the plume top, derived from radiosonde data and plume-top temperatures in the opaque regions, was found to be between 7.5 and 8.5 km, while the plume thickness was estimated to be between 1.5 and 3 km. Cloud height derived from ATSR-2 stereoscopy on a different plume gave heights in the range 5 to 8 km.

The results of this study provide important information on the optical properties of nascent volcanic eruption plumes. This information may prove useful in determining the potential effects of volcanic clouds on local climate, and in assessing any hazard to aviation.

KEYWORDS: Aviation hazards Volcanic eruptions

1. INTRODUCTION

Explosive emissions from active volcanoes are of interest to scientists and aviation authorities because they have effects on local and global climate and because they can disrupt airline traffic. The adverse effects of ash particles rich in silica (SiO_2) on the operation of jet turbine engines has been recognized for some time (see Casadevall 1994 and references therein), and several encounters between jet aircraft and ash clouds have resulted in significant engine damage and threat to life. There is also great potential for the disruption of regular air traffic routes from volcanic activity; increased awareness of this problem has resulted in the establishment of a world-wide network of volcanic ash advisory centres.

Gaseous emissions from volcanoes, principally SO_2 and water vapour, can cause effects on climate through formation of sulphuric acid, which in high enough concentrations can alter the radiation balance of the atmosphere. Sulphuric acid particles resident in the stratosphere reflect short-wave radiation to space and increase the planetary albedo; these aerosols also absorb infrared radiation. Volcanic ash particles can also affect the radiation balance. Gerstell *et al.* (1995) have shown that heating rates due to volcanic ash can exceed 20 K day^{-1} and that the amplitude of the heating is sensitive to the mean ash particle radius. However, the large particles tend to fall out relatively quickly†, and usually the radiative effects due to large (radii >5 μm) ash particles are not global. Knowledge concerning the effects of volcanoes on climate has been gained from the recent large eruptions of Pinatubo, El Chichón, and Mt St Helens (e.g. Newell

* Corresponding author: CSIRO, Atmospheric Research, Aspendale, Victoria, Australia.
e-mail: Fred.Prata@dar.csiro.au

† The time taken for ash particles to fall from 20 to 5 km can be up to a month for spherical particles with radii $\approx$5 μm, but several times longer for some other shapes (Wilson and Huang 1979).

and Deepak 1982; Hansen *et al.* 1992; McCormick *et al.* 1995; Fiocco *et al.* 1996; Self *et al.* 1996), but much less is known of the numerous moderate sized eruptions (Volcanic Explosivity Index ≈ 2), which occur on average once every few weeks somewhere on the earth (Simkin and Siebert 1994). Information on the size distribution of particles from these eruptions is needed to assess the importance of volcanic ash on the local climate and to evaluate its potential as a natural hazard (e.g. to jet aircraft and human health). Such data would also be useful in trajectory modelling of the dispersal of ash plumes (e.g. Searcy *et al.* 1998), since it is now known that vertical separation of the lighter gaseous constituents and heavier particulates occurs (Holasek *et al.* 1996), often leading to different trajectories. Ash particles and gaseous emissions from volcanic eruptions are also known to have chronic and acute effects on the human eye and respiratory system (Buist and Bernstein 1986 and references therein). There are very few quantitative measurements of the characteristics of ash clouds and ash plumes and this study is directed at providing some of this information.

Several authors (Hanstrum and Watson 1983; Sawada 1987; Prata 1989a,b; Holasek and Rose 1991; Kinoshita *et al.* 1992; Stowe *et al.* 1992; Baran *et al.* 1993; Grainger *et al.* 1993; Wen and Rose 1994; Ackerman and Strabala 1994; Holasek and Self 1995; Schneider *et al.* 1999, among others) have developed methods for using satellite data, particularly from AVHRR-2*, to quantify the properties of ash clouds. A recent overview of the use of meteorological satellite data in volcanological studies is given by Oppenheimer (1998).

A widely accepted method for detecting silica-rich ash constituents in clouds is the reverse absorption method first proposed by Prata (1989a). The principle of the method relies on a thermal infrared spectral signature, due to silicate particles, being fundamentally different to the thermal signatures of water and ice. In many circumstances the method can be used to unambiguously distinguish silica-bearing ash constituents from water or ice constituents in the atmosphere. In this work, we use this unique signature together with a radiative transfer model to derive particle size information in a silica-rich ash plume from eruptions of Mt Ruapehu in New Zealand, during June and July 1996. Our analysis follows that of Wen and Rose (1994) and we describe the accuracy and limitations of the methodology. To augment our analyses we use a cloud-shadow technique to determine the height of the cloud edge, some ancillary meteorological data combined with satellite radiances, and independent cloud stereoscopic information to estimate cloud-top heights. Combination of the geometrical properties of the cloud and the particle size determinations allow us to estimate mass loadings. A new spectral discrimination technique is presented using data from the visible and near-infrared channels of the ATSR-2. We also suggest how data from the new generation of earth observing sensors (e.g. AATSR/MERIS, GLI, MODIS, MTSAT, SEVIRI) might be used to improve the analysis and provide the benefit of near real-time hazard warning for the aviation industry.

The paper is organised as follows: first we briefly describe the volcanological setting for the June and July 1996 Mt Ruapehu eruptions. Next, we introduce the satellite datasets and discuss their spectral and spatial characteristics. The quantitative deductions concerning the satellite-retrieved microphysics and morphology of the ash cloud follow, but the mathematical details are provided in a separate report (Prata and Grant 2001). The new spectral discrimination technique is introduced and the optical properties of a volcanic cloud model are presented. The paper concludes with a

* See the appendix for a list of acronyms used in this paper.

discussion of the potential of these techniques for near real-time detection of hazardous ash clouds from current and proposed earth observing satellites.

2. Mt Ruapehu eruptions of June–July 1996

Mt Ruapehu (39.28°S, 175.57°E) on the North Island of New Zealand, is a large ($\approx$110 km^3), active, andesite–dacite volcano (Hackett and Houghton 1989). A detailed narrative of the June and July 1996 Ruapehu eruptions is given by Bryan and Sherburn (1999). The eruption phases and level of activity are inferred from seismic records. The activity during June and July is divided into several phases, each containing several volcanic earthquakes, sometimes accompanied by small to medium sized eruptions. At around 0600 LT (local time, LT = UTC + 12 hours) on 17 June 1996 Ruapehu began erupting, and clouds were first observed at about 0650 LT (Smithsonian Institution 1996). Intermittent activity continued throughout the morning and by 1500 LT the volcano was erupting every 15 minutes or so. These eruptions produced a plume of ash that extended several hundred kilometres towards the north-east. The height of the plume was estimated to be 2–3 km above the main vent (summit elevation is 2.797 km), although the Smithsonian Institution (1996) reported heights of 20 km* around 1512 LT, 17 June 1996. Light ash falls were reported to the north of the volcano up to the Bay of Plenty, more than 200 km from the volcano, and at Tauranga and Whakatane on the Bay of Plenty coast (see Fig. 7 for locations). Domestic flights to and from the North Island were suspended and airline authorities declared a danger zone surrounding the mountain, prohibiting flying in darkness around Ruapehu. At Rotorua, a popular tourist centre, a visiting Scottish rugby team is reported to have called off a practice because ash was irritating players' eyes. At Turangi, a small town to the north of Ruapehu, residents were advised to stay indoors, or wear face protection (e.g. a mask or a damp cloth) if outside, to avoid inhaling the ash.

Further eruptions took place during the evening and over the next few days. On 19 June, there were reports of aircraft encountering ash clouds from Mt Ruapehu as they approached Auckland (36.88°S, 174.75°E). Two international airports were eventually closed.

The July activity was similar in nature to the June eruptions with frequent small eruptions and columns extending several kilometres above the vent. Bryan and Sherburn (1999) report that there were continuous tremors, volcanic earthquakes and an ash eruption to 5 km elevation.

The composition of the eruptives from past and recent Ruapehu eruptions has been studied by Gamble *et al.* (1999); they found that the SiO_2 content of samples from the 1996 eruptions was about 57%. The petrology and mineral chemistry of Ruapehu volcano lava and tephra for the period 1945–96 generally indicates high silica content (>55%), consistent with andesitic ejecta.

The main data for this study come from the AVHRR-2 instrument carried on board the NOAA operational polar orbiting satellites and the ATSR-2 carried on board the ERS-2 polar orbiting satellite. The AVHRR-2 has been used in numerous applications, and a technical description of the instrument may be found in Planet (1988). The AVHRR-2 carries two visible channels with bandpass wavelengths (bandwidths) of 0.58–0.68 μm and 0.725–1.1 μm, and three infrared channels with bandwidths of 3.55–3.93, 10.3–11.3 and 11.5–12.5 μm. The linear pixel size at nadir is approximately 1 km. AVHRR-2 images are obtained in real-time from a local receiving station operated by

* Our analysis will show that this height estimate is in error and that the plume height was certainly no greater than 10 km.

CSIRO in Hobart (42.9°S, 145.6°E), Australia. The digital counts corresponding to the five channels are demultiplexed, calibrated and converted to visible reflectances or thermal brightness temperatures, in accordance with the most recent methods described in various technical memoranda published by NOAA (e.g. Planet 1988; Rao *et al.* 1993). Accurate navigation is performed using an orbit model in combination with geographical ground control points that permit pixels to be navigated to approximately 1 km precision.

The ATSR-2 is a conically scanning visible and infrared filter radiometer in polar orbit on board the ERS-2 satellite. The bandwidths and bandcentres (in brackets) of the channels are: 0.545–0.565 (0.55) μm, 0.649–0.668 (0.66) μm, 0.855–0.875 (0.87) μm, 1.55–1.65 (1.61) μm, 3.53–3.93 (3.7) μm, 10.3–11.3 (10.8) μm and 11.5–12.5 (12.0) μm. The offset conically scanning mirror provides two views (within about 2 minutes) of the same point on the ground at zenith angles ranging from 0° to 23° in the nadir scan, and 52° to 55° in the forward scan. The instrument is calibrated using onboard calibration systems in the visible and the infrared. The ATSR-2 has a superior digitization to the AVHRR-2 (12 bit vs. 10 bit), better calibration and better noise equivalent temperatures for the thermal channels. Its longer repeat cycle (approximately three days vs. one day) and narrower swath width (500 km vs. 2500 km) make it less useful than the AVHRR-2 for monitoring sporadic events such as volcanic eruptions. Further details of the ATSR-2 may be found in Mutlow (1999), and a detailed description of the image products and processing is given by Bailey (1995).

Four images, one from the ATSR-2 and three from the AVHRR-2, are examined in detail here. The first AVHRR-2 image was acquired at 0306 UTC (1506 LT) 17 June 1996. The second and third AVHRR-2 images were acquired at 1440 and 1909 LT 8 July 1996, and the ATSR-2 image was acquired at 1040 LT 8 July 1996. To augment the analyses, the retrieval procedure was applied to several other small plumes captured in AVHRR-2 images, from 17 to 19 June 1996.

3. ASH CLOUD DETECTION

Silica-bearing ash clouds can be discriminated from water/ice clouds by comparing the brightness temperatures in two nearby infrared window channels. The essential feature of this signature is that, at wavelengths between 8 and 14 μm, silicate particles absorb infrared radiation more strongly at shorter wavelengths, while water droplets, water vapour and ice particles (the most common constituents of meteorological clouds) absorb more strongly at longer wavelengths. Many particulates ejected from vigorous volcanic eruptions have compositions with a high silica content.

The detection technique consists of deriving top-of-atmosphere brightness temperatures from AVHRR-2 channels 4 (10.8 μm) and 5 (11.9 μm), hereafter referred to as T_4 and T_5, and constructing two-dimensional histograms for regions of interest. Theoretical analysis (e.g. Prata 1989b), radiative transfer modelling (e.g. Wen and Rose 1994) and satellite-based experimental studies (e.g. Prata 1989a) have shown that for water/ice clouds the difference in brightness temperature between T_4 and T_5 is positive, while for silica-bearing clouds the difference is negative. A plot of $T_4 - T_5$ versus T_4 (or T_5) shows a characteristic arch shape for water/ice clouds (e.g. Parol *et al.* 1991) and a distorted U-shape for silica-bearing (ash) clouds. Thus a discriminant for ash clouds is

$$T_4 - T_5 < T_{\text{cut-off}}. \tag{1}$$

In ideal circumstances $T_{\text{cut-off}}$ should be 0 K, but because of calibration uncertainties, field-of-view misalignment and mixed pixel effects, the value of $T_{\text{cut-off}}$ is chosen to be in

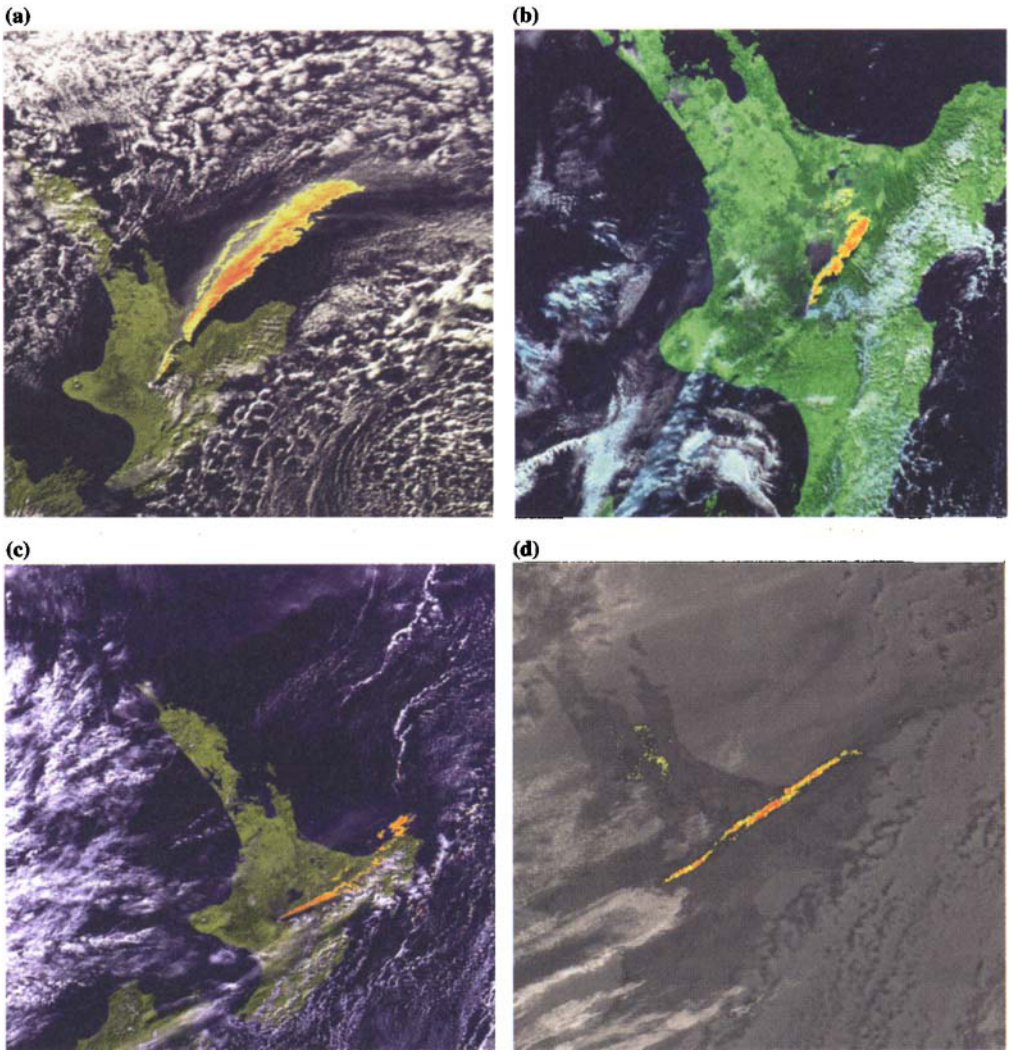

Figure 1. (a) Ruapehu plume identified in AVHRR-2 data at 1506 LT (local time, LT = UTC + 12 h) on 17 June 1996. (b) Plume identified in ATSR-2 data at 1040 LT on 8 July 1996. (c) Plume identified in AVHRR-2 at 1440 LT on 8 July 1996. (d) Plume identified in AVHRR-2 at 1909 LT on 8 July 1996. Reddest regions correspond to the most negative temperature differences, T (11 μm)–T (12 μm). A false-colour enhancement using the visible channels (1 and 2 for AVHRR-2 and the 0.67 μm and 0.87 μm channels in the case of the ATSR-2) has been used for the daytime images. See appendix for acronyms.

the range −0.5 K to +0.5 K. Figure 1(a)–(c) shows a sequence of multispectral daytime images of the Mt Ruapehu plume discriminated using condition (1) with $T_{\text{cut-off}} = 0.5$ K.

All pixels in the images were tested using condition (1); those that passed the condition were assigned a red-to-yellow colour based on the pixel's exact value of $T_4 - T_5$ (the reddest pixels correspond to the most negative differences). Figure 1(d) shows a night-time AVHRR-2 image of an ash plume also discriminated using condition (1), but with a cut-off of −0.3 K. The lower value of the cut-off is chosen because experience has shown that at night over cloud-free land $T_4 - T_5$ can be slightly negative. The yellow coloured regions on land to the north-west of the main plume are regions of cloud-free land. This analysis indicates which clouds are predominantly silica-bearing

and which are not. At the edges of the (discriminated) ash cloud there is likely to be significant mixing with ambient air which, in all likelihood, contains water vapour and/or water droplets. Therefore at the edges it is probable that pixels contain both ash and water droplets in varying amounts leading to misidentification. Thus the precise identification of the edge of the plume will always be problematic using this technique, and from a safety point of view the location of the ash cloud boundary should be treated with large uncertainty. The precise value to use for the cut-off is difficult to determine because water vapour effects tend to cancel the negative differences. Thus for operational detection of volcanic ash using this method an estimate of the water vapour effect is required. Currently we are developing a detection method that employs a water vapour correction and allows an estimate of the fraction of ash in the pixel to be determined. This research will be reported in a future paper.

In the most opaque parts of the cloud, the temperature differences tend to 0 K as the cloud starts to behave as a grey-body. This behaviour excludes the possibility of unambiguous identification of silicate particles. These regions can be used to determine cloud-top height using ancillary data (see later).

Similar comments can be made about the use of the thermal channels of the ATSR-2 as condition (1) is largely insensitive to the precise position of the bands (within the 10–12 μm window), and only slightly sensitive to the bandwidths and band overlap between channels. There is a much greater sensitivity to the noise characteristics of the channels and to their digitization. Noise becomes a particularly serious problem at low ash cloud loadings because the discriminator relies on the difference between two measurements. A final comment must be made concerning the use of the 11 and 12 μm ATSR-2 channels, which is related to the way the data are stored in the data collection system (DCS). Data bandwidth limitations with the DCS limit the number of bits used for encoding the ATSR-2 channels. These bandwidth considerations only affect the ATSR-2 daytime data; at night, full 12-bit encoding is used for the split-window channels. During the daytime, because the principal scientific objective of the ATSR-2 is to provide high precision estimates of sea surface temperatures, it was decided to use 12 bits to encode the 11 μm channel and use the remaining 8 bits to encode the difference between the 11 and 12 μm channels. This technique of bit encoding has no impact on sea surface temperature derivation because the 11–12 μm difference is nearly always positive and its dynamic range generally does not exceed 8 bits. For volcanic ash detection the technique puts constraints on the largest negative differences observable.

4. QUANTITATIVE ANALYSIS OF THE ERUPTION CLOUDS

Multispectral AVHRR-2 and ATSR-2 data can be used in a variety of ways to infer properties of ash clouds. In principle it is possible to retrieve five independent pieces of information by utilizing all of the channels available on the AVHRR-2 instrument. By combining the satellite data with ancillary measurements or by applying constraints, for example by using a radiative transfer model, it is possible to derive more than five quantities. In this work, the satellite radiances are combined with meteorological data (radiosonde profiles), a radiative transfer model and viewing information (solar and satellite view angles) to determine cloud-top height, particle sizes, cloud-base height and mass loadings. Implicit in the analysis is the determination of cloud-top temperature for opaque regions and brightness temperatures for semi-transparent regions. A plane-parallel cloud model with scattering and absorption, consisting of spherical particles with log-normal and modified-γ particle size distributions, is used to analyse the transfer of infrared radiation through the cloud to the satellite.

The quantitative analysis is based on the thermal signature identification in the satellite data. The limitations of this identification have been discussed by Prata (1989b), Barton *et al.* (1992) and Wen and Rose (1994). For particles with radii greater than 8 μm or so, the discrimination is inaccurate and ambiguities arise with water droplets and ice particles. Additionally, when the cloud becomes optically thick the detection sensitivity is poor because the temperature contrast between the (usually) warm surface and cold cloud top diminishes. For these reasons, quantitative analysis can only be performed for particles in the size range $1 < r < 8$ μm, where r is the particle radius. Although this represents only a small fraction of the total mass of ejecta from a typical eruption, it is particles in this size range that cause most damage to aircraft engines (Przedpelski and Casadevall 1994). Particles with radii less than about 10 μm are thought to pose a health hazard to the human respiratory system (e.g. see Buist and Bernstein 1986) and can also cause irritation to the eyes.

(*a*) *Ash cloud discrimination*

Wen and Rose (1994) have developed a method to determine particle sizes from AVHRR-2 channels 4 and 5. In highly simplified form, the principle of the method can be demonstrated by the following argument. Suppose that the radiances can be linearized to brightness temperatures, and that at the satellite these quantities have the values T_4 and T_5 for channels situated at approximately 11 μm and 12 μm, respectively. Suppose also that the cloud top has a temperature T_c, that the cloud is semi-transparent and that the surface below behaves as a black-body radiator with temperature T_s, with $T_s > T_c$. Denoting the emissivities of the cloud at 11 μm and 12 μm as ϵ_4 and ϵ_5, respectively, we may write

$$T_4 = \epsilon_4 T_c + (1 - \epsilon_4) T_s, \tag{2}$$

$$T_5 = \epsilon_5 T_c + (1 - \epsilon_5) T_s. \tag{3}$$

Assuming that scattering effects of the cloud particles are negligible, then

$$\epsilon_i = 1 - \exp(-k_i L), \tag{4}$$

where k_i is the absorption coefficient for channel i, and L is the geometric thickness of the cloud. Manipulating these equations and setting

$$\beta = \frac{k_5}{k_4},$$

we obtain

$$\Delta T = \Delta T_c (X - X^{\beta}), \tag{5}$$

where $X = 1 - \Delta T_4 / \Delta T_c$, $\Delta T = T_4 - T_5$, $\Delta T_c = T_s - T_c$, $\Delta T_4 = T_s - T_4$.

It is instructive to examine (5) for the cases when $\beta < 1$, $\beta > 1$, and $\beta = 1$. Plots of ΔT vs. T_4 are illustrated in Fig. 2 for these cases. It can be seen that the cases $\beta < 1$ and $\beta > 1$ lead to opposite curvatures.

This result is the basis for discriminating volcanic ash clouds from water/ice clouds by utilizing a plot of the temperature difference between AVHRR-2 channels 4 and 5 against AVHRR-2 channel 4 temperature. This plot is a two-dimensional histogram for the set of discrete measurements made from a satellite instrument such as the AVHRR-2 or ATSR-2. For ash clouds, the absorption coefficient at 11 μm is less than that at 12 μm, while the opposite is the case for water/ice clouds. This simple analysis also

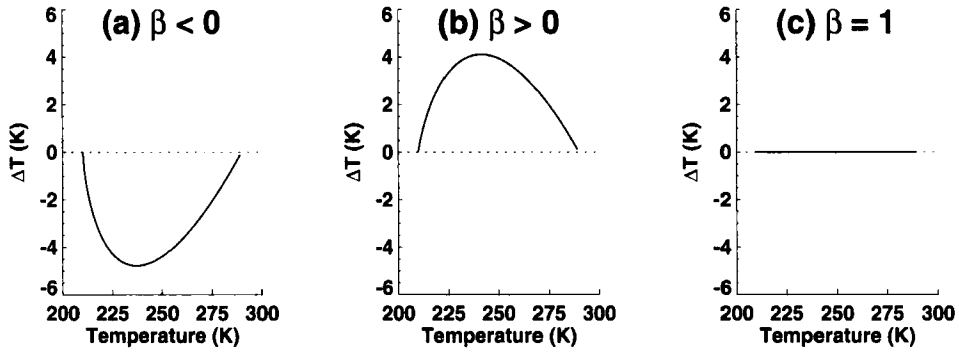

Figure 2. (a) Illustration of the 'reverse' absorption effect for volcanic ash clouds; (b) the brightness temperature difference expected for water/ice clouds; (c) when the cloud behaves non-dispersively, the brightness temperature difference is zero. See text for discussion.

shows that for clouds with a low temperature contrast ($\Delta T_c \approx 0$) discrimination from the shape of the curve is difficult or impossible. A more complete analysis shows that it is the ratio of extinction coefficients (absorption and scattering) that determines the shape of the curve.

Wen and Rose (1994) have shown that the shape of the curve depends on the mean particle size, particle size distribution, particle shape, the transparency of the cloud, and the cloud-top and surface temperatures. Particle shape may have a significant effect on the accuracy of the retrieved parameters, and future research will explore the sensitivity of the retrieval to assumed particle shape. We follow Wen and Rose and attempt to retrieve particle sizes using AVHRR-2 T_4 and T_5 brightness temperatures constrained by a radiative transfer model that includes absorption and scattering in a plane-parallel cloud.

(*b*) *Radiative transfer modelling*

Given the real and imaginary parts of the index of refraction of the ash-cloud particle as a function of wavelength, and the particle shape and size distribution, the efficiencies for scattering, absorption and extinction are calculated using a Mie-scattering program. There is scant information on particle shapes in real ash clouds, and only approximate methods exist for calculating efficiencies for particles of arbitrary shapes. We assume that the particles are spherical, and the exact Mie-theory computer program of Evans (1988) is employed to calculate the efficiencies. Some measurements exist for the particle size distribution at the edges of the Mt St Helens ash cloud (see the papers in Newell and Deepak 1982). These data indicate that a log–normal (or Zold) size distribution gives a reasonable fit to this distribution. The measurements of the El Chichón stratospheric aerosol layer reported by King *et al.* (1984) and Hoffman and Rosen (1984) fit a modified-γ size distribution quite well. These data generally pertain to volcanic aerosol layers that are relatively old and high in the atmosphere. For this work, where only the fine particles can be detected in the nascent and low (tropospheric) volcanic plumes, we assume that the size distributions would be similar. We used both size distributions to perform the radiative transfer calculations and, although there were differences in detail between the results for the two distributions, the basic results and mass loadings were essentially the same.

The parameters used in the Mie program are described in Prata (1989b) and a more complete description of the radiative transfer modelling is given in Prata and Grant

(2001). Once the Mie program has been run for each value of the size parameter (mean particle size and monochromatic wavelength), scattering parameters are fed into a plane-parallel discrete-ordinates radiative transfer program (Stamnes and Swanson 1981). Given the single scattering albedo, asymmetry parameter, extinction and scattering efficiencies as a function of monochromatic wavelength, and the cloud-top and surface temperatures, radiances emerging from the top of the cloud along n distinct streams (zenith angles) are computed. These radiances are calculated for cloud optical depths ranging from 0 to 20 at wavelengths corresponding to AVHRR-2 channels 4 and 5, and ATSR-2 11 μm and 12 μm channels. At the completion of these calculations, a large two-dimensional look-up table exists with entries at prescribed values of the mean particle size r_m and optical depth τ. Each entry in the table consists of pairs of brightness temperatures T_4 and T_5. The retrieval then consists of locating the (r_m, τ) pairs within the look-up table that best match (T_4, T_5) pairs of AVHRR-2 or ATSR-2 measurements at each image pixel.

The calculations were performed assuming that there is no absorption of infrared radiation by water vapour. This is not correct, but the effect of water vapour absorption on the results is small for the volcanic plumes studied here. The effects of atmospheric water vapour absorption on the satellite brightness temperatures have been assessed by performing radiative transfer calculations. The radiative transfer model MODTRAN 3 (Berk *et al.* 1989) was used to calculate the temperature difference between the satellite measured brightness temperatures at 11 μm and 12 μm wavelengths, at each vertical level, using the temperature and moisture structure from a nearby radiosonde profile. The effect of water vapour is greatest at the lowest levels, where it exceeds 1 K. At higher levels, near to the location of the plume, the effect is less than 0.2 K. In the tropics and in high-humidity conditions, the effect of water vapour absorption can mask out the 'reverse' absorption effect of volcanic ash clouds. This can lead to misidentification of volcanic clouds and is a limitation of the current thermal detection method. Research is being carried out to develop a method that accounts for the water vapour absorption in high-humidity conditions (Rose and Prata 1997), and will be reported in a future paper.

(*c*) *Particle radius retrievals*

Three daytime AVHRR-2 images and one ATSR-2 image were analysed in detail for the June and July 1996 eruptions of Mt Ruapehu. Figure 3 shows a contour plot of mean particle radius retrieved from the AVHRR-2 image shown in Fig. 1(a). The largest particles (up to $\approx$4 μm radii) are found around the middle of the plume and in 'clumps' distributed non-uniformly along the plume.

Some large particles found at the edges may be an artefact of the analysis because these regions are quite transparent and, as explained previously, it is possible that the entrainment of ambient (water-rich) air may be significant. There are, however, closed contours within the plume with congregations of large particles. There appears to be an elongation of the particle size contours in the direction of the wind at that level. There also appears to be a gradient in particle size from the smallest particles in the south-eastern side of the plume, to the largest particles in the north-western side of the plume.

Figure 4 shows the frequency distribution of particle sizes in the plumes for both size distribution models. Particle sizes vary from 1 to $\approx$4 μm, with mode maxima near 3 μm. There is some evidence of multiple modes within the distribution; such behaviour has been found for the Fuego and Santiago ash clouds (Cadle *et al.* 1979), the Mt St Helens ash cloud (Chuan *et al.* 1981; Farlow *et al.* 1981), and the Agung ash clouds (Mossop 1964). Chuan *et al.* (1981) found a mode peak at radius $\approx$2.5 μm when monitoring continuous emissions from Mt St Helens, prior to a strong eruption on

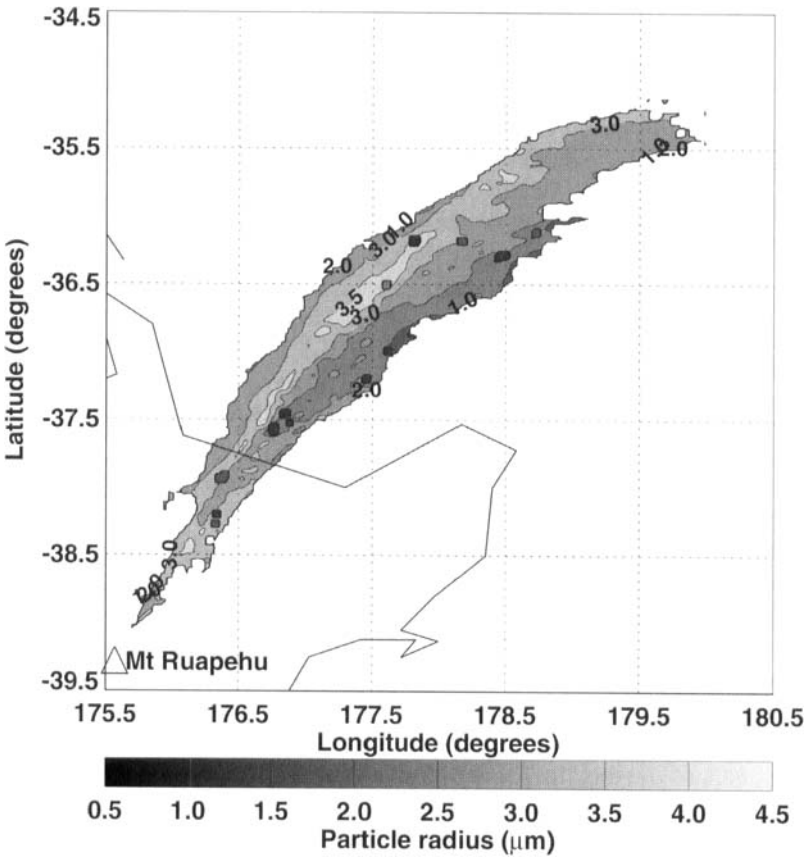

Figure 3. Contours of mean ash particle radius for the eruption of Mt Ruapehu on 17 June 1996 retrieved from the AVHRR-2 (see appendix) image in Fig. 1(a).

August 7 1980. Rose *et al.* (2000) have summarized the available direct sampling data on volcanic clouds.

(*d*) *Cloud height determination*

(i) *Cloud-top temperature/temperature profile method.* Cloud-top height can be determined by using the cloud-top temperature of opaque parts of the cloud as a proxy for the ambient temperature at the same height as the cloud top. A nearby radiosonde profile is then used to determine the height in the profile where the temperature best matches the cloud-top temperature. This method can work well provided the cloud behaves as a black-body and the radiosonde profile is representative. For high clouds near the tropopause, the method is prone to error because the rate of change of temperature with height is small and this leads to indeterminacy in the height assignment. The plume (see Fig. 3) was highlighted by selecting only those regions for which $T_4 - T_5 < +0.5$ K. The coldest parts of the plume have temperatures in the range -32 to -38 °C. It is reasonable to expect that the cloud is not behaving as a black-body (see, for example Platt and Stephens 1980), so the air temperature at the top of the cloud might be expected to be a few K lower.

Radiosonde data were obtained from the CRI, New Zealand (Burgess, personal communication) for two upper-air stations, at Whenauapi (36.47°S, 174.38°E) and

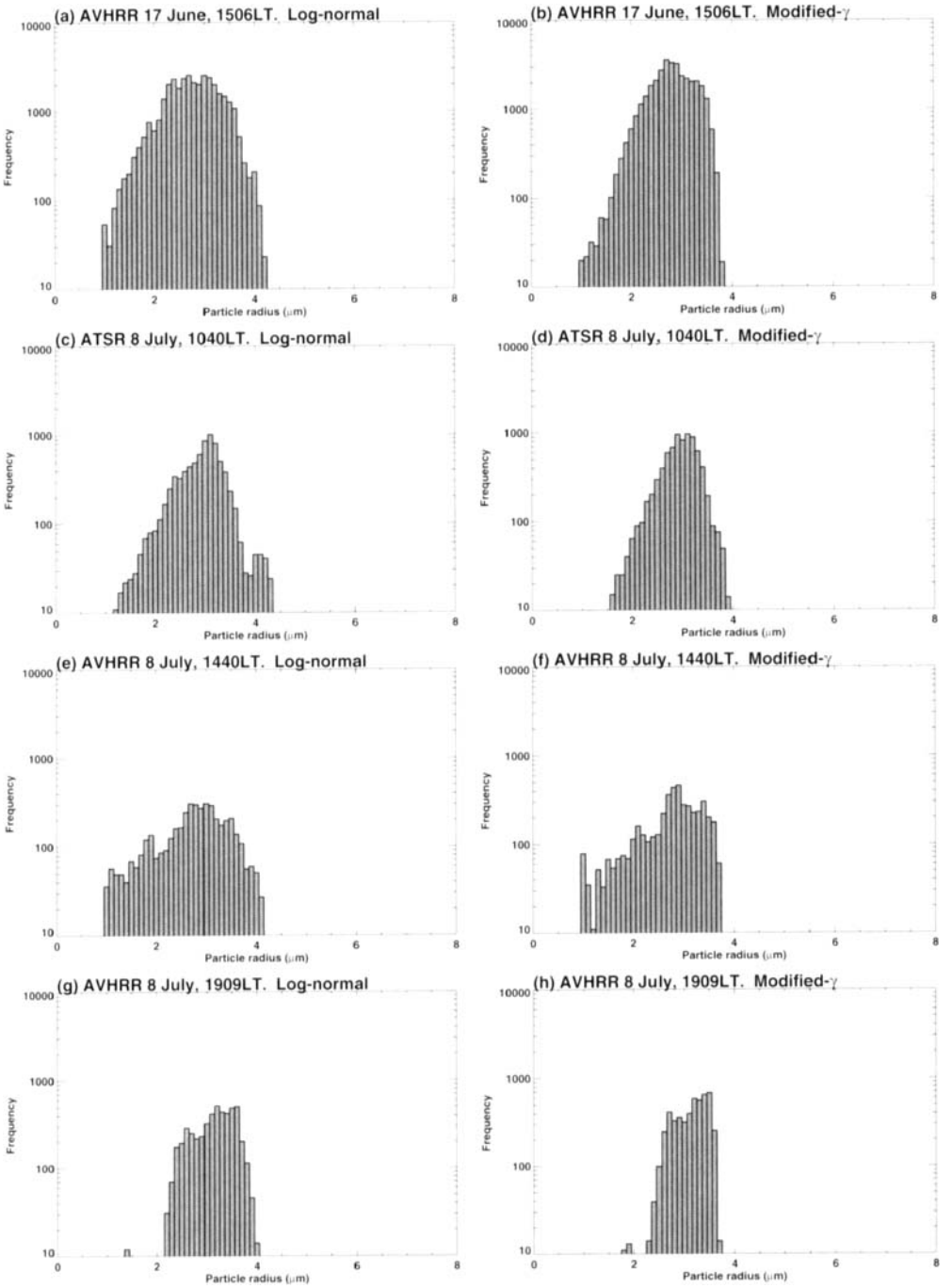

Figure 4. Histograms of retrieved particle size for four Ruapehu plumes and two model size distributions. See text for details.

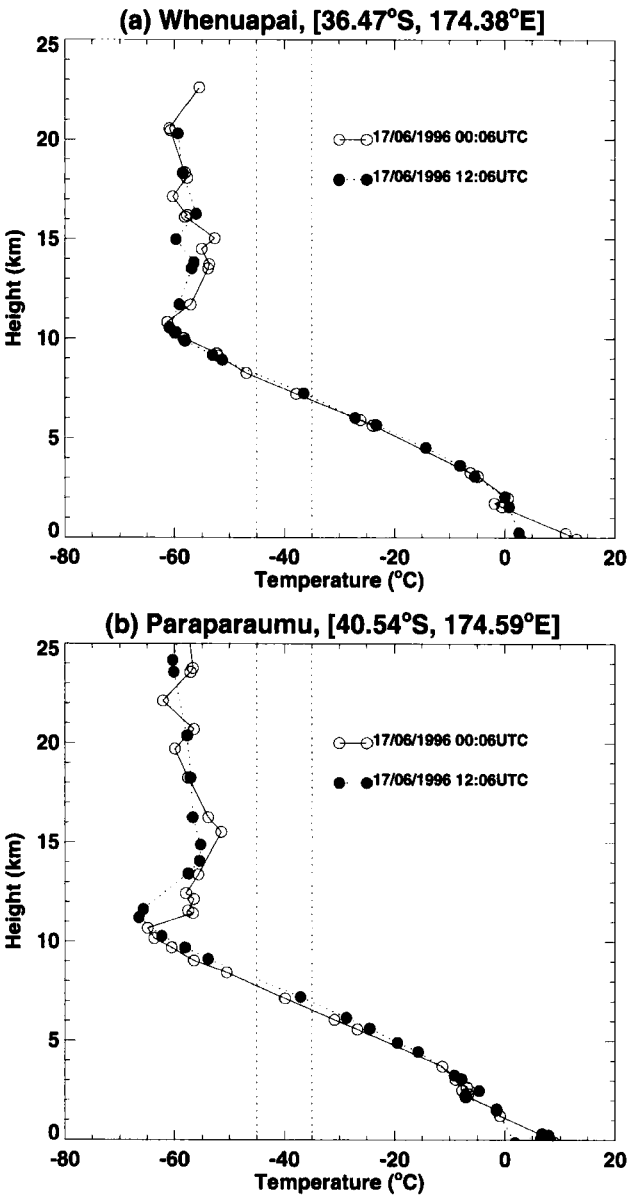

Figure 5. New Zealand radiosonde profiles for 17 June 1996.

Paraparaumu (40.54°S, 174.59°E). Launches were made at approximately 0000 and 1200 UTC 17 June 1996. Figure 5(a) and (b) show the vertical temperature profiles at Whenauapi and Paraparaumu, respectively, at 0000 and 1200 UTC on 17 June. The vertical dotted lines on the plots indicate temperatures of −35 and −45 °C, which cover the range of opaque cloud-top temperatures observed in the AVHRR image. These temperatures translate to heights of 7.5–8.5 km. Radiosonde data from both places and for the other days, give substantially the same results. Indeed it is sufficient to use the mean monthly profiles in this analysis, because the lapse rate is not varying strongly

during this time in this height range of the atmosphere. (Note that this may not have been the case had the plume been higher, or lower, in the atmosphere.)

The plumes of 8 July observed in ATSR-2 and in AVHRR-2 imagery indicate that in the most opaque regions the coldest parts of the cloud were −20 to −25 °C. These temperatures translate to cloud-top heights of about 5–6 km.

(ii) *Cloud stereoscopy.* Prata and Turner (1997) have developed an algorithm for determining cloud heights from the parallax formed between the ATSR forward and nadir views of clouds. The method is capable of accuracies of ≈1 km in height and was used to determine plume height in the ATSR-2 image of 8 July. The stereoscopic retrieval gives heights of ≈8 km for downwind points, and 5.5 km for points near to the vent (cf. heights of 5–6 km from the brightness-temperature method). Height retrievals along the length of the plume suggest a slight rise of the plume from about 5 km near to the vent to about 8 km downwind.

(iii) *Height from plume shadow.* The AVHRR-2 image of 17 June lends itself to a determination of plume height morphology from the shadow cast on the underlying surface. The method used to determine the plume height is applied separately for portions over the sea and over the land. The three-dimensional locus of the plume edge was determined from the plume and shadow edges in the AVHRR channel 1 and 2 images. The edges of the plume and shadow were extracted as contours of constant radiance, from the channel 1 and 2 images over ocean and land respectively. Each contour used roughly corresponded to the steepest gradient in radiance. Over the ocean, corresponding points on the plume and shadow edges are joined by lines at a constant azimuth that may be calculated from the view and sun directions. Over land, the apparent location of points on the shadow edge may be shifted to account for topography, so that the ocean constant-azimuth result can be used to associate shadow edge and plume edge points. The detailed description of the methods used is given in Prata and Grant (2001). Figure 6 shows a close-up channel 1 (visible) view of a part of the AVHRR-2 image of the Mt Ruapehu plume obtained on 17 June 1996. Where the plume crosses the North Island of New Zealand there is a distinct darkening of the channel 1 reflectance. This shadow can also be detected over the ocean when the image data are suitably enhanced. Since the time and the position of each pixel are available it is straightforward to obtain the relevant solar and satellite viewing angles required to compute the height of the illuminated edge of the plume. The morphology of real plumes is likely to be quite complex and it is difficult to calculate the precise part of the cloud that is responsible for the shadow.

Figure 6 also shows the retrieval of height of the plume edge (top panel), and corresponding locations of the edge and its shadow as determined on the AVHRR-2 image. As described in Prata and Grant (2001) the height retrieved by this method is, strictly speaking, that of the plume edge (Glaze *et al.* 1999). We expect this height to correspond more closely with the lower part of the plume, and represent a lower bound on the plume height and an upper bound on the plume base. The plume edge height varies from values as small as 2 km, up to just over 8 km some 200 km downwind of the vent.

(*e*) *Mass loadings*

The US military consider mass loadings >50 mg m^{-3} a potential hazard to their aircraft operations. Przedpelski and Casadevall (1994) estimated a mass loading of ≈2000 mg m^{-3} at 25 000 ft (≈7.5 km) for the 15 December 1989 Redoubt eruption

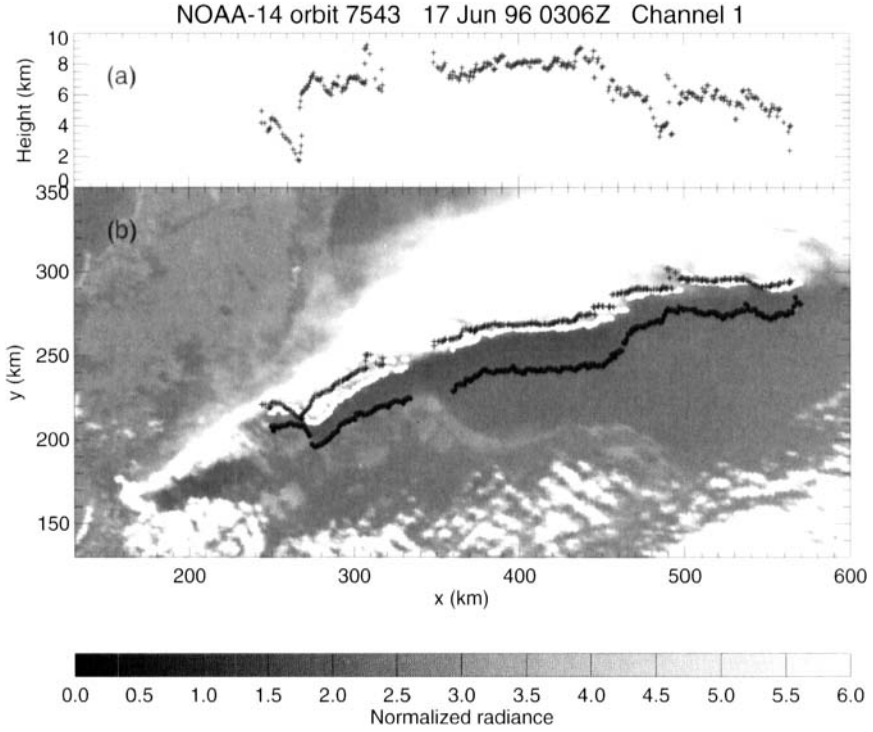

Figure 6. Close-up channel 1 (visible) view of part of the AVHRR-2 (see appendix) image of the Mt Ruapehu plume obtained on 17 June 1996. (a) The calculated height of the plume edge. (b) The AVHRR channel 1 image, rotated so that the y-axis is in the azimuth $\phi_\Delta = 153°$. The white points are taken as the plume edge and the black points as the shadow edge. The '+' symbols show the vertical projection of the calculated true plume edge; that is, the plume edge where it would be imaged by a nadir-viewing satellite.

cloud that caused significant damage to a KLM Boeing 747-400 jet aircraft. Mass loadings include all particles with radii <50 μm which have atmospheric residence times of the order of at least a few hours. Having determined the particle size distribution, the geometrical thickness of the cloud and its areal extent, it is possible to estimate the mass loading of fine particles in each of the plumes studied here. The density of the ash is taken to be 2600 kg m^{-3} and the area of a pixel is taken as 1.2 × 1.2 km^2—this is a mean area for pixels for both the AVHRR-2 and ATSR-2. Pixels are counted if they satisfy criterion (1), and the retrieved particle size is in the range $1 < r_m < 8$ μm. An estimate of the cloud thickness is crucial to the evaluation of mass loadings. Data on cloud thicknesses are not available so they must be estimated by other means. Studies of plume rise in stable stratified atmospheres (e.g. Briggs 1975) suggest that to a reasonable approximation the vertical extent of a plume can be estimated from the cloud-top height. For example, Manins (1985) has calculated the heights and vertical extents of stabilized smoke plumes as a function of power release and, following Briggs (1975), suggests that the vertical extent (cloud thickness), Δz, of these plumes is given by

$$\Delta z = 0.4 z_{top},$$

where z_{top} is the height of the plume top. The cloud-top heights calculated previously for the Ruapehu plumes suggest a cloud thickness range of 1.5–3.0 km, with a likely error of ±0.5 km. The variability of cloud thickness along the plumes, and the problem of not having simultaneous plume-top height and plume-base height data for each of the

TABLE 1. RETRIEVED MASS LOADINGS AND MODE RADII FOR THE TWO SIZE DISTRIBUTIONS USED AND FOR FOUR RUAPEHU PLUMES

		Size distribution			
		Log-normal		Modified-γ	
Date:Time	Sensor	Mass loading (mg m^{-3})	Mode radius (μm)	Mass loading (mg m^{-3})	Mode radius (μm)
17-06-96:1506	AVHRR-2	3.5–6.9	2.7	3.2–6.3	2.7
08-07-96:1040	ATSR-2	1.4–2.7	3.1	1.4–2.6	3.1
08-07-96:1440	AVHRR-2	1.5–2.9	3.0	1.4–2.6	2.9
08-07-96:1909	AVHRR-2	1.7–3.2	3.2	1.5–2.9	3.5

The range of mass loadings shown corresponds to a range in cloud thickness from 1.5 to 3.0 km.

plumes, means that we cannot estimate plume thickness to any greater accuracy. The mass loading (kg m^{-3}) is

$$M = \frac{4\pi}{3}\rho \int_o^\infty r^3 n(r)\, dr, \tag{6}$$

where ρ is the density of the ash and $n(r)$ is the size distribution. The total mass can be calculated by multiplying (6) by the volume of a pixel (geometric thickness multiplied by the area of a pixel). Table 1 lists the results obtained for all four plumes using both size distributions.

The retrievals for the plumes of 8 July should be comparable, as the time difference between the AVHRR-2 and ATSR-2 data acquisitions is not long (less than five hours) and the eruptions during these days were similar in nature. The mode radii on all days are similar, but the mass loading differences between the June eruption and the July events are probably significant.

Hobbs *et al.* (1981) made aircraft-based measurements of the size distributions and number densities of ash in the periphery of the Mt St Helens plume. Some measurements were made at 3 km altitude and 9.3 km downwind of the volcano, and these can be compared with our results. For particles in the size range 1–5 μm, the number density is of the order 1–10 cm^{-3} (see Fig. 2(b) of Hobbs *et al.* 1981), which correspond to mass loadings of 0.1–1.0 mg m^{-3}. Sehmel (1982) also reported mass loadings in the range 1–10 mg m^{-3} in the dispersed Mt St Helens volcanic cloud. Our results may also be compared with silicate mass loading retrievals by Yu and Rose (2000) for the El Chichón clouds, and from recent estimates made by W. I. Rose (personal communication) for the June–September 1992 Spurr eruptions. These mass loadings were found to be in the range 1–5 mg m^{-3}. Wen and Rose (1994) determined the total mass of fine particles for the 19 August 1992 Crater Peak/Spurr eruption and obtained a value of 0.2×10^6 t. They estimated the cloud area to be 10^5 km^2, giving a mass loading range of 1.5–3.0 mg m^{-3} for a cloud thickness range of 1.5–3.0 km. Wen and Rose also show that their total mass estimates are not significantly affected by the choice of size distribution.

The mean retrieved mass loadings are an order of magnitude smaller than the value considered hazardous to aircraft (cf. $\approx$50 mg m^{-3} or greater). The mass loadings calculated here represent only those particles in the restricted size range $1 < r < 8$ μm, and these represent only a small fraction of the total mass of ejected matter. However, these are the particles which are most hazardous to jet engines, and it would appear to be necessary to develop a mass loading threshold based on particles in this size range. It is also likely that most of the larger particles will have fallen out soon after an eruption.

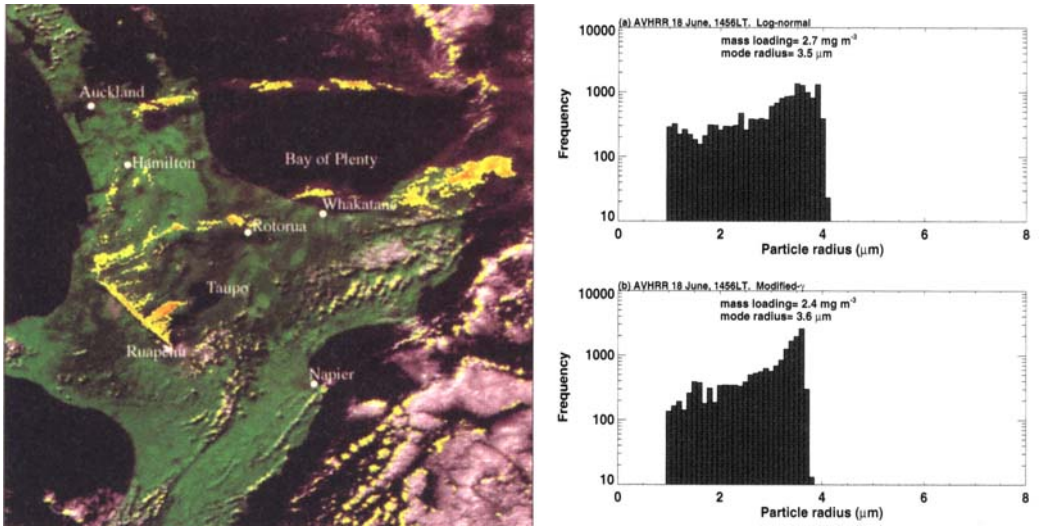

Figure 7. AVHRR-2 (see appendix) image acquired at 1456 LT (local time, LT = UTC + 12 h) on 18 June 1996. The image size is 500 km × 500 km. Ash clouds are coloured red to yellow. The locations of some towns with domestic airports are indicated on the image. There is an international airport at Auckland. The right-hand panel shows particle size distributions retrieved for these plumes, (a) log-normal size distribution, (b) modified-γ size distribution.

The mass in the fine-ash size range typically represents ≈1% of the total mass ejected (e.g. Wen and Rose 1994; Bursik *et al.* 1994). Rose *et al.* (2000) found that the fine-ash percentages in volcanic clouds represented between 0.04 and 2.6% of the total erupted mass. Using a typical figure of 1% suggests a *total* mass loading of 100–500 mg m^{-3} for the Ruapehu clouds and thus they would have been a threat to jet aircraft.

To examine whether this kind of information could be of value to aviation, we also obtained AVHRR-2 data for 18 June 1996, just 24 hours after the eruption responsible for the large plume of 17 June. The ash clouds are discriminated using the reverse absorption effect with a cut-off of −0.25 K. Particle size retrievals were made for an area of about 500 × 500 km^2, covering most of the North Island of New Zealand. Figure 7 shows the results of this analysis. The plume has apparently bifurcated with two branches to the north of Lake Taupo spreading eastwards and over the Bay of Plenty. Flights to and from the North Island were suspended, closing the domestic airports at Rotorua, Hamilton, Tauranga and Whakatane. Ash falls were reported along the Bay of Plenty coast from Taurangi to Whakatane. It can be seen that some edges of clouds have also been diagnosed as ash-bearing (e.g. the cloud edges to the east of Napier). We believe these are not ash clouds, but are probably occuring because of slight misalignments of the centres of the fields-of-view of the 11 μm and 12 μm channels. Choosing a more negative cut-off temperature does eliminate these anomalies but also reduces the sensitivity of detection of ash-bearing plumes.

The mass loadings and particle size retrievals for this image are shown in Fig. 7. Evidently the mass loadings are still significant, but there is a suggestion from the histogram of greater concentrations of particle sizes at the small-size end of the distribution ($r \approx 1$ μm). Note that retrievals below 1 μm have not been attempted because of the lack of sensitivity of the technique. This information was not available at the time of these events, but we believe that the locations of the ash plumes on the image shown

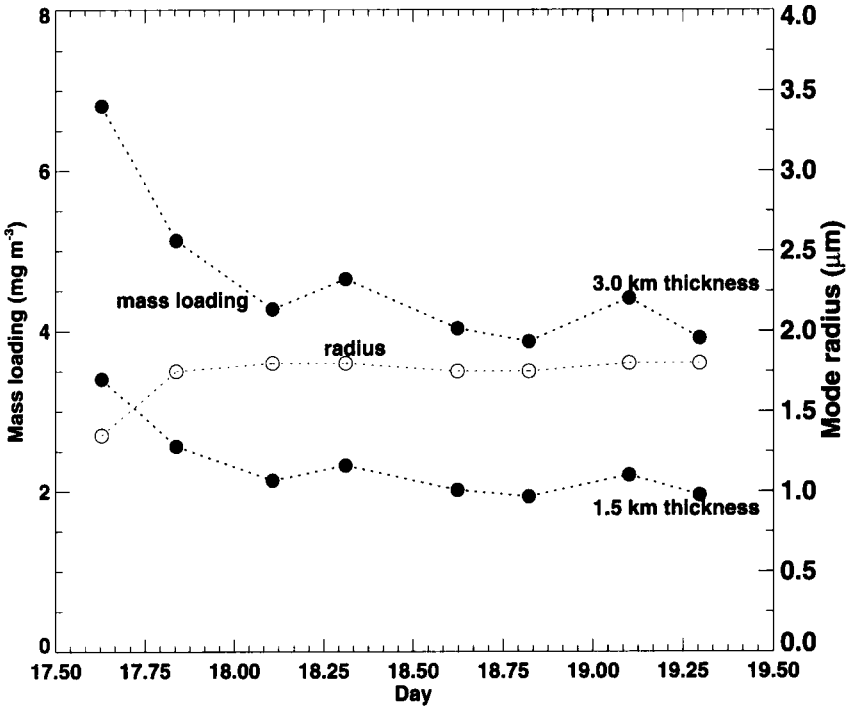

Figure 8. Mass loading and mode radius as a function of time for the 17–19 June 1996 Ruapehu plumes. See text for details.

in Fig. 7 and the mass loading retrievals are consistent with independent observations of the plumes and the actions taken by the civil aviation authority in closing the North Island airports. This kind of information, together with conventional meteorological data (e.g. wind speed and direction) and trajectory forecasts, would give aviation authorities greater confidence in their advice to air traffic concerning the ash cloud hazard.

It is also of interest to know how long the suspended ash remains in the atmosphere and the rate of decay of the size distribution with time. Bursik *et al.* (1994) have calculated the settling velocities for different ash grain sizes, with an initial concentration related to plume height. In their model the time taken for the concentration of 5.5 μm diameter grains to decrease by exp(−1) of the initial concentration, which is also the time taken for each grain to fall a distance of 5 km under static conditions, is found to be about 23 days. For 11 μm diameter grains the settling time is 4.8 days. In our study the mode radius is close to 3.5 μm and the settling time would be about 8 days. The temporal evolution of the retrieved mass loading and mode radius based on satellite data for the Ruapehu plumes of 17–19 June is plotted in Fig. 8. After a rapid decrease in mass loading and increase in mode radius, the plumes have relatively constant properties. The oscillations in the mass loading retrievals may be a manifestation of error in the assumed thickness of the plumes, which we assumed to be 1.5–3.0 km. An exponential decay of the mass loading does not fit these data well, but the retrievals are consistent with residence times of several days, rather than several hours.

TABLE 2. REFRACTIVE INDICES (REAL PART n_r, IMAGINARY PART n_i) FOR WATER, ICE AND ANDESITE (A SILICA-RICH MINERAL) WITH REFERENCES

Wavelength (μm)	n_r	n_i	Reference
Ice			
0.63	1.309	1.04×10^{-8}	Masuda and Takashima (1990)
1.61	1.289	3.41×10^{-4}	
Water			
0.63	1.332	1.44×10^{-8}	Masuda and Takashima (1990)
1.61	1.317	0.87×10^{-4}	
Andesite			
0.68	1.470	1.70×10^{-3}	Pollack *et al.* (1973)
1.61	1.470	3.30×10^{-3}	

5. DETECTION IN THE VISIBLE AND NEAR INFRARED

It has been explained that the two-channel thermal infrared discrimination technique fails when the cloud is optically thick. Usually this is not of concern because most plumes 'thin out' towards their edges, allowing increased chance of detection at the plume edges. However, there are occasions when detection at the edges is difficult. Problems occur in humid atmospheres (e.g. in the tropics) when the positive difference in brightness temperature due to water vapour absorption masks the negative difference due to the ash, or when entrainment of water-rich ambient air dilutes the ash component.

The ATSR-2 has three visible channels and one near-infrared channel that can provide complementary cloud microphysical information to the thermal channels. At visible wavelengths ($\lambda < 0.8$ μm) water and ice clouds tend to scatter radiation rather than absorb it. Narrow-band, directional radiance measurements of ash clouds from the ATSR-2 are difficult to interpret because changing illumination and viewing conditions lead to a range of possible reflectances. It is not straightforward to assign a reflectance threshold for ash cloud detection because the same cloud may appear darker or brighter depending on the particular viewing conditions. The same arguments apply to water/ice clouds and these clouds can appear as dark as, or darker than, ash clouds, depending on viewing and illumination conditions.

(*a*) *Volcanic cloud model*

At near-infrared wavelengths (e.g. $\lambda = 1.61$ μm) ice clouds appear much darker than clouds of water droplets, because the imaginary part of the refractive index of ice is larger than that of water at this wavelength, and consequently ice absorbs more strongly at this wavelength. A comparison of the refractive indices of water, ice and andesite (a common constituent of ash clouds) is given in Table 2.

Pollack *et al.* (1973) list refractive indices of andesite (and some other minerals) over a large range of wavelengths from the ultraviolet to the infrared. These data are not the only source of refractive index values for minerals; see for example, Volz (1973), Ivlev and Popova (1973) and Sokolik and Toon (1999). We have used the Pollack *et al.* values as a starting point to provide the input optical parameters required for more detailed radiative transfer calculations, and we propose a model of a volcanic ash cloud based on the Pollack *et al.* refractive indices of andesite. The ash cloud model consists of spherical andesite particles in a log-normal size distribution with a mean particle radius of 3 μm. The single-scatter albedo, asymmetry parameter and coefficients of absorption, scattering and extinction are calculated for the polydisperse particle size distribution

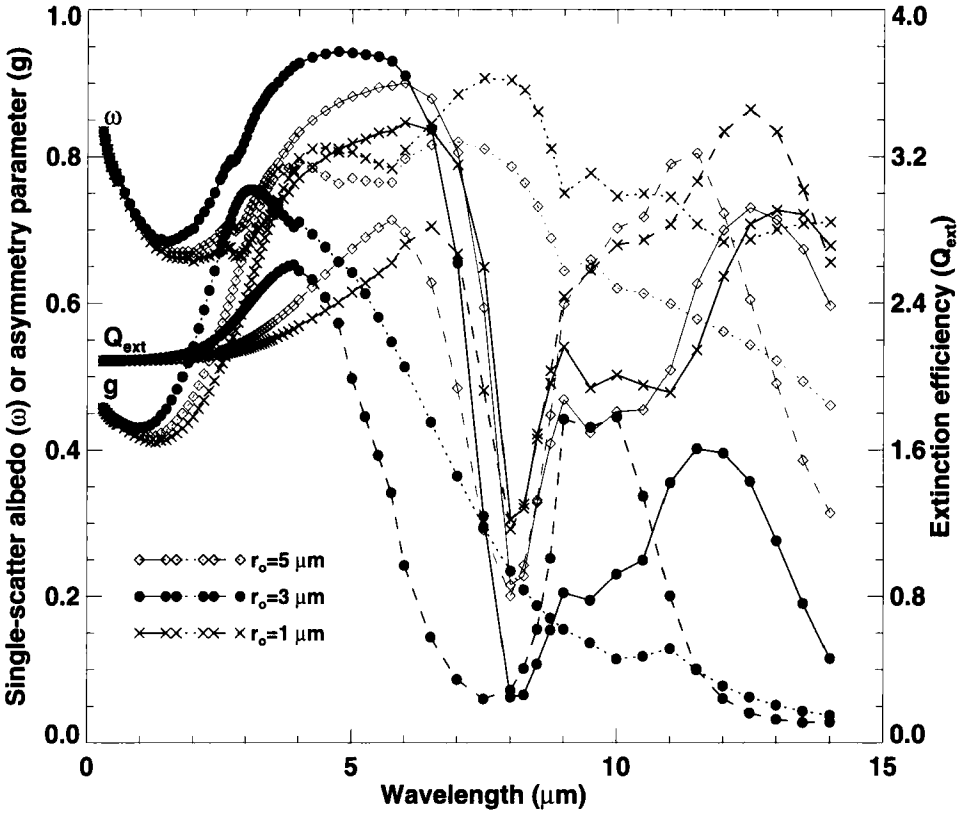

Figure 9. Optical parameters: single-scatter albedo, ω, extinction coefficient, Q_{ext}, and asymmetry parameter (g) for the andesite volcanic ash cloud model. The wavelength range is 0.3 μm to 14.5 μm and results for three mean particle radii (r_o) are shown.

using the Mie program discussed earlier. Figure 9 shows the variation of single-scatter albedo (ϖ), extinction coefficient (Q_{ext}), and asymmetry parameter (g) for wavelengths ranging from 0.3 μm to 14.5 μm, the range most commonly used in remote sensing of the earth's atmosphere. The results for a model ash cloud with mean particle radii of 1, 3, and 5 μm are shown.

(*b*) *Visible and near-infrared detection algorithm*

Table 2 shows that ash absorbs more at visible wavelengths (0.63–0.68 μm) than both water and ice, and that the imaginary part of the refractive index of ash is almost five orders of magnitude greater than water and ice at these wavelengths. At near-infrared wavelengths, ash absorbs more strongly than ice and water, and ice absorbs more strongly than water. We argue therefore, that a ratio of visible to near-infrared reflectances, or vice versa, should provide a means of distinguishing clouds predominantly of ash from those predominantly of water/ice. The purpose of using the ratio is to eliminate, to a large degree, variations in illumination and viewing conditions and provide an objective discriminator.

In order to verify this reasoning, radiative transfer calculations were performed for the ATSR-2 0.67 μm and 1.61 μm channels using the water/ice cloud models of Stephens (1979) and the ash cloud model developed in this work.

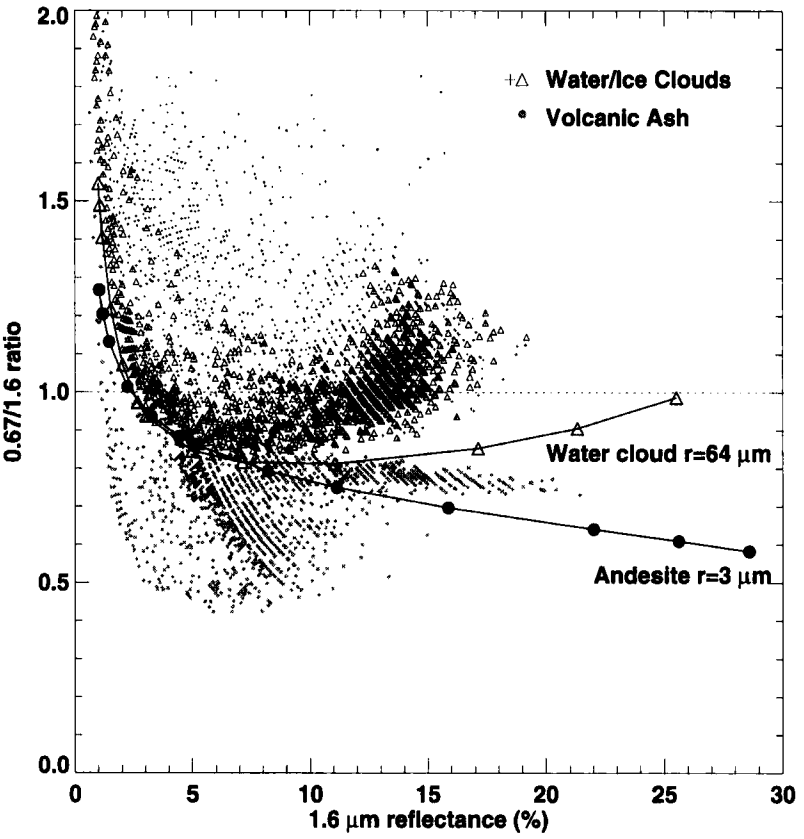

Figure 10. Ratio of reflectances at 0.67 μm to 1.6 μm versus 1.6 μm reflectance for the Ruapehu plume of 8 July 1996. Radiative transfer calculations are indicated by the continuous lines; •—andesite cloud model, and △—water cloud model.

Calculations were performed for a variety of illumination and viewing conditions and for two water cloud models (Stephens 1979), one ice cloud model (Hunt 1973), the andesite ash cloud model, and for clouds consisting of pure quartz particles and sulphuric acid droplets (Palmer and Williams 1975). The results indicate that the ratio does discriminate ash from water/ice clouds, and that the discrimination is greatest at largest optical depth. The results are illustrated in Fig. 10, which shows the radiative transfer calculations overlayed onto ATSR-2 measurements of the Ruapehu plume on 8 July 1996. The abscissa is the 1.6 μm reflectance and the ordinate is the ratio of visible to near-infrared reflectance. Increasing values of 1.6 μm reflectance imply increasing optical depth.

These results suggest that the reflectance ratio may be a useful adjunct to the thermal discrimination technique, although this complementarity can only be exploited for daylight hours. The technique appears to work best in the parts of the cloud that are most opaque. Use of the visible, near-infrared and thermal channels together would seem to offer the best strategy for extracting ash cloud properties from satellite radiances. Extrapolating further, there would appear to be some interesting possibilities for such studies using the advanced multispectral sensors GLI, MODIS, AATSR/MERIS, MTSAT and SEVIRI.

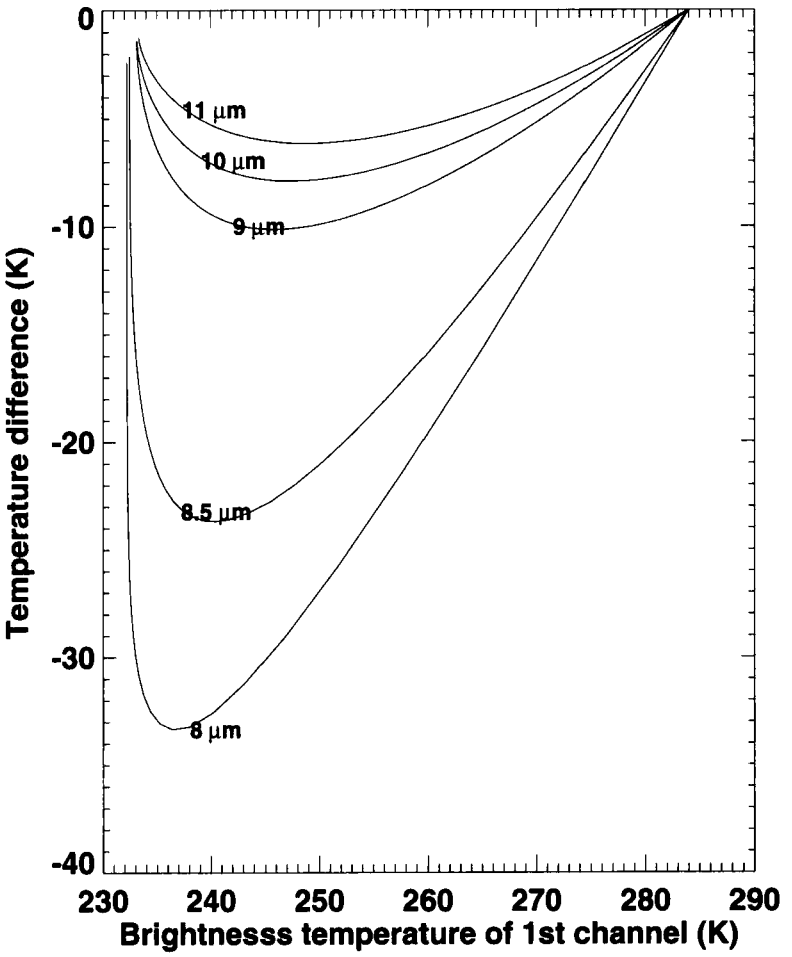

Figure 11. Temperature difference vs. temperature curves for combinations of infrared channels, with a 12 μm channel as the reference channel. Greatest sensitivity (largest negative temperature differences) occurs when the second channel has the shortest wavelength.

(*c*) *Enhanced thermal detection*

The new sensors also have greater multispectral capability in the thermal infrared and can be used to provide an enhanced 'reverse' absorption signature for volcanic ash detection. It is beyond the scope of this paper to examine all of the nuances involved in extracting information on volcanic cloud constituents from multispectral thermal data, but a straightforward demonstration of the potential for an enhanced thermal detection algorithm is presented in Fig. 11. This shows the brightness temperature difference obtained using a channel centred at 12 μm, differenced with channels centred at shorter wavelengths of 8.0, 8.5, 9.0, 10.0 and 11.0 μm.

The calculations were performed, as before, using the discrete-ordinates radiative transfer model and the optical properties of the 'idealized' andesite cloud model. It is clearly evident that channels centred around 8.5 μm and 12 μm would provide a much stronger anomaly (larger negative temperature differences) than the present 11 and 12 μm channels. Some of the new sensors have such a channel combination (e.g. MODIS, GLI and SEVIRI). Moreover, previous studies using these channels show

that water/ice clouds also have much larger positive temperature differences, which suggests that the enhanced algorithm will provide greater sensitivity to clouds with mixed constituents (water/ice and ash) and to volcanic clouds with low ash loadings. The effects of water vapour have not been considered, and these effects will reduce the magnitude of the negative temperature difference because there is more water vapour absorption at 8.5 μm than at 11 μm.

6. CONCLUSIONS

We have developed and tested a scheme to determine the mean particle radius of fine particles, the optical depth, cloud-top height and mass loadings of some Ruapehu volcanic clouds using satellite data. The fine particles have the longest atmospheric residence times and it is therefore important to estimate their mass contribution to the atmosphere. The retrieved parameters will provide useful information to aviation authorities; mass loading of silicates in dispersing plumes is essential information required to assess the hazard to jet aircraft. The size distributions and masses of fine particles determined from the retrieval algorithm suggest that these plumes cause mass loadings in the range $\approx$1 to $\approx$7 mg m^{-3}, comparable with estimates for other dispersed volcanic clouds. The parameters may also be useful in studies of the radiative effects of volcanic eruptions on the earth–atmosphere climate system and for ash plume trajectory modelling. The results found here agree with previous studies, which indicate that there are numerous short-lived particles with radii less than a few microns in small to moderate sized eruption plumes. While these plumes may not have any impact on global climate, their local effects are of concern.

The Ruapehu volcanic clouds were easily identified in the infrared channels of the AVHRR-2 and ATSR-2, and this may have been a result of earlier eruptions (17 September 1995), which ejected most of the water from the lake at the crater, leaving subsequent eruptions relatively free of water. In many other volcanic clouds we have examined, unambiguous identification of silicate ash by the reverse absorption effect has been masked by interstitial water and/or ice. Rose *et al.* (1995) showed that ice in the eruption cloud of the September 1996 Rabaul eruption completely masked the thermal signature.

We have also discovered a new method for detecting airborne volcanic substances by utilizing information of their scattering properties in the visible and near-infrared. Volcanic plumes with large amounts of ash (e.g. with silicate particles) can be discriminated from water/ice clouds at large optical depth (near infrared reflectances larger than 10% or so) by a 'ratioing' technique. The method relies on the observation that, at wavelengths near 0.67 μm and 1.6 μm, ash particles absorb radiation in similar amounts, whilst water and ice are about 1000 times more absorbing at 1.6 μm than at 0.67 μm. Currently, there are just a few satellite-borne sensors that can take advantage of this, but the advanced sensors, AATSR/MERIS, MODIS, GLI and SEVIRI will have multiple wavebands in the visible and near-infrared that may be used to exploit this new method. Ideally, for an operational warning system, a constellation of at least five multispectral instruments capable of rapid imaging in geosynchronous orbit above the earth would provide a most suitable means for volcanic ash detection. Based on comparisons of GOES, GMS-5, AVHRR-2 and ATSR-2 instruments, a spatial resolution of 1 km^2 (or better) and a noise equivalent temperature difference (NEΔT) of 0.05 K (or better) at 300 K are required for 0.5–1 μm-width channels at central wavelengths of 8.6, 10.8 and 12.0 μm. Low NEΔTs are necessary because the detection technique relies on using temperature differences at sometimes low (<250 K) target temperatures. However, it

needs to be stressed that in the early stages of the development of an eruption it is unlikely that the reverse absorption technique described here will provide an effective discrimination method. This may not be of vital importance to aviation because common sense suggests that *any* clouds occurring close to a volcano that is in eruption should be avoided. For research purposes, space-borne infrared interferometers have the potential to provide new information on the radiative effects of volcanic substances (particulates and gases). Nadir and limb viewing interferometers on polar orbiters will provide complementary information, likely to greatly enhance our understanding of the physics, chemistry and dynamics of volcanic clouds. Two previous satellite-based studies (Prata 1989a; Barton *et al.* 1992) have suggested that sulphuric acid droplets (liquid phase) and SO_2 gas may also yield a thermal signature similar to that of silica-rich ash clouds. Baran *et al.* (1993) and Grainger *et al.* (1993) have used satellite radiances to study sulphuric acid aerosols in the stratosphere, and Realmuto *et al.* (1994) have shown that it is possible to determine SO_2 column amounts from thermal radiances in the 8–13 μm window. Thus multispectral remote-sensing instruments such as hyperspectral spectrometers in the visible and Fourier Transform Infrared interferometers (e.g. ENVISAT/MIPAS and GIFTS) in the thermal wavelengthas can be exploited to retrieve information on a variety of volcanic constituents.

APPENDIX

List of acronyms

AATSR	Advanced Along-Track Scanning Radiometer
ATSR	Along-Track Scanning Radiometer
AVHRR	Advanced Very High Resolution Radiometer
CRI	Crown Research Institute
CSIRO	Commonwealth Scientific and Industrial Research Organisation
DEM	Digital Elevation Model
ENVISAT	Environmental Satellite
ERS	European Remote-sensing Satellite
GIFTS	Geostationary Imaging Fourier Transform Spectrometer
GLI	Global Imager
GMS	Geostationary Meteorological Satellite
GOES	Geostationary Operational Environmental Satellite
GVN	Global Volcanism Network
MERIS	Medium Resolution Imaging Spectrometer
MIPAS	Michelson Interferometer for Passive Atmospheric Sounding
MODIS	Moderate resolution Imaging Spectroradiometer
MTSAT	Meteorological Satellite
NOAA	National Oceanographic and Atmospheric Administration
SEVIRI	Spinning Enhanced Visible Infrared Imager
VAAC	Volcanic Ash Advisory Centre

REFERENCES

Ackerman, S. A. and Strabala, K. I. 1994 Satellite remote sensing of H_2SO_4 aerosol using the 8 to 12 μm window region: Application to Mount Pinatubo. *J. Geophys. Res.*, **99**(D9), 18639–18649

Bailey, P. 1995 'SADIST-2 v100 Products'. Rutherford Appleton Laboratory Report, ER-TN-RAL-AT-2164, Space Science Department, RAL, Didcot, Oxon., UK

Baran, A. J., Foot, J. S. and Dibben, P. C. 1993 Satellite detection of volcanic sulphuric acid aerosol. *Geophys. Res. Lett.*, **20,** 1799–1801

Barton, I. J., Prata, A. J., Watterson, I. G. and Young, S. A. 1992 Identification of the Mt Hudson volcanic cloud over SE Australia. *Geophys. Res. Lett.*, **19,** 1211–1214

Berk, A., Bernstein, L. S. and Robertson, D. C. 1989 'MODTRAN: A moderate resolution model for LOWTRAN 7. AFGL-TR-89-0122'. US Air Force Phillips Laboratory, Nascom Air Force Base, MA, USA

Briggs, G. A. 1975 Plume rise predictions. Pp. 59–111 in *Lectures on air pollution and environmental impact analyses*. American Meteorological Society, Boston, USA

Bryan, C. J. and Sherburn, S. 1999 Seismicity associated with the 1995–1996 eruptions of Ruapehu volcano, New Zealand: Narrative and insights into physical processes. *J. Volcanol. Geotherm. Res.*, **90,** 118

Buist, A. S. and Bernstein, R. S. (Eds.) 1986 Health effects of volcanoes: An approach to evaluating the health effects of an environmental hazard. *Am. J. Public Health–Supplement*, **76,** 90 pp.

Bursik, M. I., Sparks, R. S. J., Carey, S. N. and Gilbert, J. S. 1994 'The concentration of ash in volcanic plumes, inferred from dispersal data. Pp. 19–29 in Proceedings of the first international symposium on volcanic ash and aviation safety, July 1991. US Geological Survey Bulletin 2047, Seattle, Washington, USA

Cadle, R. D., Lazrus, A. L., Huebert, B. J., Heidt, L. E., Rose, W. I. Jr., Woods, D. C., Chuan, R. L., Stoiber, R. E., Smith, D. B. and Zielinski, R. A. 1979 Atmospheric implications of studies of Central American volcanic eruption clouds. *J. Geophys. Res.*, **84**(C11), 6961–6968

Casadevall, T. J. (Ed.) 1994 'Volcanic ash and aviation safety'. Proceedings of the first international symposium on volcanic ash and aviation safety, July, 1991. US Geological Survey Bulletin 2047, Seattle, Washington, USA

Chuan, R. L., Woods, D. C. and McCormick, M. P. 1981 Characterisation of aerosols from eruptions of Mount St Helens. *Science*, **211,** 830–832

Evans, B. T. N. 1988 'An interactive program for estimating extinction and scattering properties of most particulate clouds'. Department of Defence Report MRL-R-1123, Defence Science and Technology Organisation, Materials Research Laboratory, PO Box 50, Ascot Vale, Victoria 3032, Australia

Farlow, H. N., Oberbeck, V. R., Snetsinger, K. G., Ferry, G. V., Polkowski, G. and Hayes, D. M. 1981 Size distributions and mineralogy of ash particles in the stratosphere from eruptions of Mt St Helens. *Science*, **211,** 832–834

Fiocco, G., Fuà, D. and Visconti, G. (Eds.) 1996 'The Mount Pinatubo eruption: Effects on the atmosphere and climate'. NATO ASI Series I: Global Environmental Change 42, Springer-Verlag, Berlin, Germany

Gamble, J. A., Wood, C. P., Price, R. C., Smith, I. E. M., Stewart, R. B. and Waight , T. 1999 A fifty year perspective of magmatic evolution on Ruapehu Volcano, New Zealand: verification of open system behaviour in an arc volcano. *Earth and Planetary Sci. Lett.*, **170,** 301–314.

Gerstell, M. F., Crisp, J. and Crisp, D. 1995 Radiative forcing of the stratosphere by SO_2 gas, silicate ash, and H_2SO_4 aerosols shortly after the 1982 eruptions of El Chichón. *J. Climate*, **8,** 1060–1070.

Glaze, L. S., Wilson, L. and Mouginis-Marks, P. J. 1999 Volcanic eruption plume top topography and heights as determined from photoclinometric analysis of satellite data. *J. Geophys. Res.*, **104**(B2), 2989–3001

Grainger, R. G., Lambert, A., Taylor, F. W., Remedios, J. J., Rodgers, C. D. and Corney, M. 1993 Infrared absorption by volcanic stratospheric aerosols observed by ISAMS. *Geophys. Res. Lett.*, **20,** 1283–1286

Hackett, W. R. and Houghton, B. F. 1989 A facies model for a Quaternary andesitic composite volcano, Ruapehu, New Zealand. *Bull. Volcanol.*, **51,** 51–68

Hansen, J., Lacis, A., Redy, R. and Sato, M. 1992 Potential climate impact of the Mount Pinatubo eruption. *Geophys. Res. Lett.*, **19,** 215–218

Hanstrum, B. N. and Watson, A. S. 1983 A case study of two eruptions of Mount Galunggung and an investigation of volcanic eruption cloud characteristics using remote sensing techniques. *Aust. Meteorol. Mag.*, **31,** 171–177

Hobbs, P. V., Radke, L. F., Eltgroth, M. W. and Hegg, D. A. 1981 Airborne studies of the emissions from the volcanic eruptions of Mount St Helens. *Science*, **211**, 816–818

Hofmann, D. J. and Rosen, J. M. 1984 Balloonborne particle counter observations of the El Chichón aerosol layers in the 0.01–1.8 μm radius range. *Geofis. Int.*, **23**, 155–185

Holasek, R. E. and Rose, W. I. 1991 Anatomy of 1986 Augustine volcano eruptions as revealed by digital AVHRR satellite imagery. *Bull. Volcanol.*, **53**, 420–435

Holasek, R. E. and Self, S. 1995 GOES weather satellite observations and measurements of the May 18, Mount St Helens eruption. *J. Geophys. Res.*, **100**, 8469–8487

Holasek, R. E., Woods, A. W. and Self, S. 1996 Experiments on gas–ash separation processes in volcanic umbrella plumes. *J. Volcanol. Geothermal Res.*, **70**, 169–181

Hunt, G. E. 1973 Radiative properties of terrestrial clouds at visible and infrared thermal window wavelengths. *Q. J. R. Meteorol. Soc.*, **99**, 356–369

Ivlev, L. S. and Popova, S. I. 1973 The complex refractive indices of substances in the atmospheric-aerosol dispersed phase. *Atmos. Oceanic Phys.*, **9**(10), 587–591

King, M. D., Harshvardhan and Arking, A. 1984 A model of the radiative properties of the El Chichón stratospheric layer. *J. Clim. Appl. Meteorol.*, **23**, 1121–1137

Kinoshita, K., Masumizu, T. and Tsutsumi, K. 1992 'Analysis of satellite images of volcanic ash clouds from Mount Sakurajima'. Pp. 2003–2008 in Proceedings of the 18th international symposium on space technology and science, Kagoshima, Japan

McCormick, M. P., Thomason, L. W. and Trepte, C. R. 1995 Atmospheric effects of the Mt Pinatubo eruption. *Nature*, **373**, 399–404

Manins, P. C. 1985 Cloud heights and stratospheric injections resulting from a thermo-nuclear war. *Atmos. Environ.*, **19**(8), 1245–1255

Masuda, K. and Takashima, T. 1990 Deriving cirrus information using the visible and near-IR channels of the future NOAA-AVHRR radiometer. *Remote Sensing Environ.*, **31**, 65–81

Mossop, S. C. 1964 Volcanic dust collected at an altitude of 20 km. *Nature*, **203**, 9, 824–827

Mutlow, C. T. 1999 'ATSR-1/2 User Guide'. Rutherford Appleton Laboratory Report, 15 June 1999 Issue 1 RAL, Didcot, Oxon, UK (Also http://www.atsr.rl.ac.uk/user_documentation.html).

Newell, R. E. and Deepak, A. (Eds.) 1982 'Mount St Helens eruptions of 1980: Atmospheric effects and potential climate impact'. NASA Workshop Report, NASA SP-458, Scientific and Technical Information Branch, NASA, Washington, DC, USA

Oppenheimer, C. 1998 Volcanological applications of meteorological satellites. *Int. J. Remote Sensing* **19**(15), 2829–2864

Palmer, K. F. and Williams, D. 1975 Optical constants of sulfuric acid: Application to the clouds of Venus? *Appl. Opt.*, **14**(1), 208–219

Parol, F., Buriez, J. C., Brogniez, G. and Fouquart, Y. 1991 Information content of AVHRR channels 4 and 5 with respect to the effective radius of cirrus cloud particles. *J. Appl. Meteorol.*, **30**, 973–984

Planet, W. G. 1988 'Data extraction and calibration of TIROS-N/NOAA radiometers'. NOAA Technical Report NESS 107–Rev. 1, National Environment, Satellite Data and Information Services, Washington, DC, USA

Platt, C. M. R. and Stephens, G. L. 1980 The interpretation of remotely sensed high cloud emittances. *J. Atmos. Sci.*, **37**, 2314–2322

Pollack, J. B., Toon, O. B. and Khare, B. N. 1973 Optical properties of some terrestrial rocks and glasses. *Icarus*, **19**, 372-389

Prata, A. J. 1989a Observations of volcanic ash clouds using AVHRR-2 radiances. *Int. J. Remote Sensing*, **10**(4-5), 751–761

1989b Radiative transfer calculations for volcanic ash clouds. *Geophys. Res. Lett.*, **16**, 1293–1296

Prata, A. J. and Grant, I. F. 2001 'Determination of mass loadings and plume heights of volcanic ash clouds from satellite data'. CSIRO Atmospheric Research Technical Paper No. 48. CSIRO, Aspendale, Victoria, Australia (http://www.csiro.au/publications/Prata_2001a.pdf)

Prata, A. J. and Turner, P. J. 1997 Cloud top height determination from the ATSR. *Remote Sensing Environ.*, **59**, 1–13

Przedpelski, Z. J. and Casadevall, T. J. 1994 'Impact of volcanic ash from 15 December 1989 Redoubt volcano eruption on GE CF6-80C2 turbofan engines'. Pp. 129–135 in Proceedings of the first international symposium on volcanic ash and aviation safety, July 1991. US Geological Survey Bulletin 2047, Seattle, Washington, USA

Rao, C. R. N., Sullivan, J. T., Walton, C. C., Brown, J. W. and Evans, R. H. 1993 'Nonlinearity corrections for the thermal infrared channels of the advanced very high resolution radiometer: Assessment and recommendations'. NOAA Technical Report NESDIS 69. National Environmental Satellite Data and Information Service, Washington, DC, USA

Realmuto, V. J, Abrams, M. J., Buongiorno, M. F. and Pieri, D. C. 1994 The use of multispectral thermal infrared image data to estimate sulfur dioxide flux from volcanoes: A case study from Mount Etna, Sicily, July 29 1986. *J. Geophys. Res.*, **99**, 481–488

Rose, W. I. and Prata, A. J. 1997 Atmospheric corrections for two band infrared volcanic cloud discriminations and retrievals. *EOS Trans. Am. Geophys. Union*, **F818**

Rose, W. I., Bluth, G. J. S. and Ernst, G. G. J. 2000 Integrating retrievals of volcanic cloud characteristics from satellite remote sensors: A summary. *Philos. Trans. R. Soc.*, London **A No. 358,** 1585–1606

Rose, W. I., Delene, D. J., Schneider, D. J., Bluth, G. J. S., Kruger, A. J., Sprod, I., McKee, C., Davies, H. L. and Ernst, G. J. 1995 Ice in the 1994 Rabaul eruption: Implications for volcanic hazard and atmospheric effects. *Nature*, **375**, 477–479

Sawada, Y. 1987 'Study on analysis of volcanic eruptions based on eruption cloud image data obtained by Geostationary Meteorological Satellite (GMS)'. Technical Report 22, Meteorological Institute of Japan, Tokyo

Schneider, D. J., Rose, W. I., Coke, L. R. and Bluth, G. J. S. 1999 Early evolution of a stratospheric volcanic eruption cloud as observed with TOMS and AVHRR. *J. Geophys. Res.*, **104**(D4), 4037–4050

Searcy, C., Dean, K. and Stringer, B. 1998 PUFF: A volcanic ash tracking and prediction model. *J. Volcanol. and Geophys. Res.*, **40**, 1–16

Sehmel, G. A. 1982 Ambient airborne solids concentrations including volcanic ash at Hanford, Washington, sampling sites subsequent to the Mount St Helens eruption. Pp. 283–392 in *Atmospheric effects and potential climatic impact of the 1980 eruptions of Mount St Helens*. Ed. Deepak. NASA Conference Publication 2240, NASA Scientific and Technical Information Branch, Washington, DC, USA

Self, S., Zhao, J-X., Holasek, R. E., Torres, R. C. and King, A. J. 1996 The atmospheric impact of the 1991 Mount Pinatubo eruption. Pp. 1089–1115 in *Fire and mud: Eruptions and lahars of Mount Pinatubo, Philippines*. Eds. C. G. Newhall and R. S. Punongnayan. Philippine Institute of Volcanology and Seismology, Queen City, Philipines and University of Washington Press, Seattle, USA

Simkin, T. and Siebert, L. 1994 *Volcanoes of the world*. Geoscience Press, Tucson, Arizona, USA

Smithsonian Institution 1996 *Bulletin of the Global Volcanism Network*. **21**(5), May 1996. Museum of Natural History, Smithsonian Institution, Washington DC, USA (http://www.nmnh.si.edu/gvp/gvn/bulletin.htm)

Sokolik, I. N. and Toon, O. B. 1999 Incorporation of mineralogical composition into models of the radiative properties of mineral aerosol from UV to IR wavelengths. *J. Geophys. Res.*, **104**(D8), 9423–9444

Stamnes, K. and Swanson, R. A. 1981 A new look at the discrete ordinates method for radiative transfer calculations in anisotropically scattering atmospheres. *J. Atmos. Sci.*, **38**, 387–399

Stephens, G. L. 1979 'Optical properties of eight water cloud types'. CSIRO Atmospheric physics technical paper No. 36, CSIRO, Aspendale, Victoria, Australia

Stowe, L. L., Carey, R . M. and Pellegrino, P. P. 1992 Monitoring the Mt Pinatubo aerosol layer with NOAA/11 AVHRR data. *Geophys. Res. Lett.*, **19**, 159–162

Volz, F. E. 1973 Infrared optical constants of ammonium sulfate, Sahara dust, volcanic pumice, and flyash. *Appl. Opt.*, **12**(3), 564–568

Wen, S. and Rose, W. I. 1994 Retrieval of sizes and total masses of particles in volcanic clouds using AVHRR bands 4 and 5. *J. Geophys. Res.*, **99**(D3), 5421–5431

Wilson, L. and Huang, T. C. 1979 The influence of shape on the atmospheric settling velocity of volcanic ash particles. *Earth and Planetary Sci. Lett.*, **44**, 311–324

Yu, T-X. and Rose, W. I. 2000 Retrieval of sulfate and silicate ash masses in young (1 to 4 days old) eruption clouds using multiband infrared HIRS/2 data. Pp. 87–110 in *Remote sensing of active volcanism.* Geophysical Monograph 116, Eds. Peter J. Mouginis-Mark, Joy A. Crisp and Jonathan H. Fink. AGU, Washington, DC, USA